GEOPHYSICAL RESEARCH LETTERS, VOL. 40, 1409–1414, doi:10.1002/grl.50287, 2013

Southern Ocean bottom water characteristics in CMIP5 models

Céline Heuzé,[1] Karen J. Heywood,[1] David P. Stevens,[2] and and Jeff K. Ridley[3]

Received 17 January 2013; revised 22 February 2013; accepted 25 February 2013; published 15 April 2013.

[1] Southern Ocean deep water properties and formation processes in climate models are indicative of their capability to simulate future climate, heat and carbon uptake, and sea level rise. Southern Ocean temperature and density averaged over 1986–2005 from 15 CMIP5 (Coupled Model Intercomparison Project Phase 5) climate models are compared with an observed climatology, focusing on bottom water. Bottom properties are reasonably accurate for half the models. Ten models create dense water on the Antarctic shelf, but it mixes with lighter water and is not exported as bottom water as in reality. Instead, most models create deep water by open ocean deep convection, a process occurring rarely in reality. Models with extensive deep convection are those with strong seasonality in sea ice. Optimum bottom properties occur in models with deep convection in the Weddell and Ross Gyres. Bottom Water formation processes are poorly represented in ocean models and are a key challenge for improving climate predictions. **Citation:** Heuzé, C., K. J. Heywood, D. P. Stevens, and J. K. Ridley (2013), Southern Ocean bottom water characteristics in CMIP5 models, *Geophys. Res. Lett.*, *40*, 1409–1414, doi:10.1002/grl.50287.

1. Introduction

[2] The Southern Ocean plays a key role in regulating the Earth's climate: it connects the three main ocean basins, transporting heat and carbon [*Séférian et al.*, 2012], and its sea ice greatly affects the planetary albedo. Bottom water formed in the Southern Ocean circulates worldwide [*Orsi et al.*, 1999].

[3] Numerous global climate models (GCMs), with different parameterizations, resolutions and structure, are being used by scientists worldwide to estimate the likely climate in 50–100 years (e.g., global temperature increase or sea level rise). The ability of a model to adequately depict bottom water formation is crucial for accurate prediction of changes in the thermohaline circulation [*Hay*, 1993]. In the real ocean, Antarctic Bottom Water usually forms when cold dense water spills off the shelf [*Orsi et al.*, 1999] and then spreads northwards. This process is particularly challenging to represent in the current generation of climate models. There have also been episodes of open ocean deep convection, mostly observed in the Weddell Sea in the 1970s [*Killworth*, 1983]. Here, we assess how dense water is formed in climate models, and how this impacts the representation of ocean properties at the sea bed.

[4] The Coupled Model Intercomparison Project Phase 5 (CMIP5) project [*Taylor et al.*, 2012] facilitates assessment of the models' ability to depict the present observed state of the climate system, a prerequisite for reliable future prediction. Southern Ocean observational data coverage has dramatically increased over recent decades, particularly in the ice-free regions, enabling a detailed analysis of climate model simulations of this key region. The last generation of models in CMIP3 poorly represented Southern Ocean transport and heat fluxes [*Russell et al.*, 2006]. Subantarctic Mode Water and Antarctic Intermediate Water layer thicknesses and northward extensions were too small, despite a reasonably accurate depiction of temperature and salinity [*Sloyan and Kamenkovich*, 2007]. To our knowledge, there has been no assessment of Antarctic Bottom Water in CMIP3 models. Here, we evaluate bottom water properties in the Southern Ocean in CMIP5 models.

2. Methodology

[5] We assess Southern Ocean potential temperature, salinity, density and sea ice concentration in 15 CMIP5 historical simulations (means of the 20 August monthly mean fields from 1986 to 2005, of the first ensemble member, designated r1i1p1 in PCMDI terminology). The models include a hybrid/isopycnal model: GFDL-ESM2G [*Dunne et al.*, 2012], available through CMIP5 on z-level coordinates, and three σ-coordinate models: INMCM4 [*Volodin et al.*, 2010] requiring conversion to z-coordinates, MIROC4h [*Sakamoto et al.*, 2012] and MIROC-ESM-CHEM [*Watanabe et al.*, 2011], both available converted to z-level coordinates. The remaining 11 are traditional z-level models: CanESM2 [*Chylek et al.*, 2011], CNRM-CM5 [*Voldoire et al.*, 2011], CSIRO-Mk3-6-0 [*Gordon et al.*, 2010], GFDL-ESM2M [*Dunne et al.*, 2012], GISS-E2-R [*Schmidt et al.*, 2006], HadGEM2-ES [*Jones et al.*, 2011], HiGEM [*Shaffrey et al.*, 2009], IPSL-CM5A-LR [*Dufresne et al.*, in revision], MPI-ESM-LR [*Jungclaus et al.*, 2010], MRI-CGCM3 [*Yukimoto et al.*, 2011] and NorESM1-M [*Tjiputra et al.*, 2012].

[6] The 20 year mean model fields are compared with historical hydrographic data on a grid spacing of 0.5° × 0.5° [*Gouretski and Koltermann*, 2004], and with the Hadley Centre sea ice climatologies [*Rayner et al.*, 2003]. The model fields have all been interpolated to the same grid as the hydrographic climatology, and the climatological values subtracted from the model fields to provide difference maps. For each model, we calculate the area-weighted root mean square (RMS) difference from the climatology of the diagnostic fields at all depths (similar results were obtained for different depth ranges); in the absence of relevant uncer-

Additional supporting information may be found in the online version of this article.

[1]School of Environmental Sciences, University of East Anglia, Norwich, UK.
[2]School of Mathematics, University of East Anglia, Norwich, UK.
[3]Met Office Hadley Centre, Exeter, UK.

Corresponding author: C. Heuzé, School of Environmental Sciences, University of East Anglia, Norwich Research Park, Norwich NR4 7TJ, UK. (c.heuze@uea.ac.uk)

0094-8276/13/10.1002/grl.50287

tainty measurements for the climatological fields, the model will be considered as accurate if for each parameter, its RMS difference is smaller than the mean RMS difference of the 15 models.

[7] The hydrographic climatology is biased towards summer observations, but this does not affect our results since bottom properties are seasonally decoupled from the surface. To estimate the climatological mixed-layer values in winter, we assume that the properties of the subsurface temperature minimum (Winter Water) represent the temperature and salinity that the mixed-layer would have had the previous winter.

[8] For all models, we calculate potential density relative to 2000 m (σ_2) and relative to the surface (σ_θ) using the equation of state EOS80 [*Fofonoff and Millard*, 1983]. Salinities are quoted on the practical salinity scale and so have no units. We analyze the properties at the deepest grid cell during the August mean, when sea ice extent is greatest and deep water forms. In considering the replenishment of deep water, we determine for each grid point for each August throughout the 20 years of the study, the maximum of the mixed-layer depth (MLD) using a density σ_θ threshold of 0.03 kg m^{-3} from the 10 m depth value (as defined by *de Boyer Montégut et al.* [2004]). The same technique is used for the climatology, using the Winter Water density as the 10 m value. To show the percentage of the water column that is well-mixed, we present the MLD divided by the water depth at each point. A value close to 100% indicates areas where deep convection occurs. We do not use the mixing parameters *mlotst* and *omlmax*, which are some of the recommended CMIP5 outputs, because they are not available for all the models. We prefer using a consistent definition for all models and the climatology. We also found that the CMIP5-recommended globally applied threshold of 0.125 kg m^{-3} was too high to correctly determine MLD in the relatively unstratified Southern Ocean. Salinity is not shown, but whether each model is too salty or too fresh can be deduced from considering the temperature and density maps together, since density depends on both temperature and salinity.

3. Results

[9] The RMS differences from the climatology for bottom temperature and density for each model are indicated on Figures 1 and 2, respectively. They can also be found in Table S1 (in the Auxiliary Material) along with the RMS differences for salinity, the area-weighted mean differences for each parameter, and the 20 year trends that we discuss at the end of this section.

[10] Bottom temperature in the whole deep Southern Ocean in locations deeper than 1000 m for CNRM-CM5 (Figure 1c), GFDL-ESM2M (Figure 1e), MPI-ESM-LR (Figure 1j), MRI-CGCM3 (Figure 1k) and MIROC4h (Figure 1o) is on average about 1°C warmer than the climatology. As their salinity fields (not shown) are within 0.05 of the climatological value in the same area and therefore do not dominate the density difference, they are less dense than the climatology by on average 0.15 kg m^{-3} (Figures 2c, 2e, 2j, 2k and 2o). In contrast, GFDL-ESM2G (Figure 1m) and INMCM4 (Figure 1n) are more than 0.5°C colder than the climatology on average for locations deeper than 1000 m in the Southern Ocean. The largest difference is encountered in the Pacific sector for INMCM4 (1.4°C colder) and in the Atlantic for GFDL-ESM2G (0.8°C colder). GFDL-ESM2G is also fresher than the climatology in the whole area (by 0.1), hence, its density is within 0.05 kg m^{-3} of the climatology on average in the Southern Ocean (Figure 2m). However, the deep waters of INMCM4 are 0.7 saltier across the entire deep Southern Ocean, and so 0.7 kg m^{-3} denser in this area (Figure 2m). CanESM2 (Figure 1b) and MIROC-ESM-CHEM (Figure 1p) temperatures lie within 0.2°C of the climatology, but are on average 0.2 saltier, so they are 0.15 kg m^{-3} denser than the climatology (Figures 2b and 2p), consistent with the dominant effect of the salinity. GISS-E2-R (Figure 1f) is on average within 0.5°C of the climatological values, but its temperature RMS difference is greater (1.24°C) because of the meridional gradient in temperature: the model displays a 6°C difference between the subtropics (50°S) and the Antarctic waters (80°S), whereas the climatology displays a maximum of 3.5°C difference over the same latitude range. The same phenomenon is observed for GISS-E2-R's salinity and density (Figure 2f). For locations deeper than 1000 m in the Southern Ocean, CSIRO-Mk3-6-0 (Figure 1d), HadGEM2-ES (Figure 1g), HiGEM (Figure 1h), IPSL-CM5A-LR (Figure 1i) and NorESM1-M (Figure 1l) are within 0.5°C and 0.1 in salinity, and is within 0.05 kg m^{-3} of the observed climatology (Figures 2d, 2g, 2h, 2i and 2l).

[11] We now consider if the source of the dense bottom water could originate from dense shelf water (Figure 2). Bottom density maps are not shown, but shelf production can be seen where areas of deep convection (inside the black contour) intersect regions shallower than 3000 m (inside the gray contours). Five models produce very little or no dense water on the shelf: CNRM-CM5 (Figure 2c), MRI-CGCM3 (Figure 2k), NorESM1-M (Figure 2l), MIROC4h (Figure 2o) and MIROC-ESM-CHEM (Figure 2p). Models have a fixed freezing point, set to values ranging from –2.5°C to –1.8°C, so the difference between the shelf temperature and the climatology has an upper limit. The water produced on the shelf is not dense enough in these models, because it is far too fresh: more than 0.25 fresher than in the deep ocean. No consistent link has been found between shelf water density and sea ice extent.

[12] The other models produce dense water on the Ross and Weddell Sea shelves, with enhanced local densities of more than 0.2 kg m^{-3}, in agreement with the climatology. However, because of the horizontal/isopycnal diffusion schemes in z-level GCMs, this dense water formed on the Antarctic shelf mixes horizontally as well as vertically at each grid point as it travels down the shelf slope. Longitudinal sections (not shown) suggest that through enhanced mixing, the dense shelf water is unable to maintain its properties while sinking and propagating northwards, becoming mixed with intermediate waters. None of the models are able to form dense bottom water through export from the continental shelf. Even though one might expect that the isopycnal (Figure 2m) or σ-coordinate (Figures 2n, 2o and 2p) models should simulate this process better, we find no evidence that these four models are any better at exporting dense water from the shelf.

[13] The climate models in this study generate dense bottom water through open ocean deep convection. In observations, this process occurs rarely [*Marshall and Schott*, 1999] and does not penetrate to the sea bed.

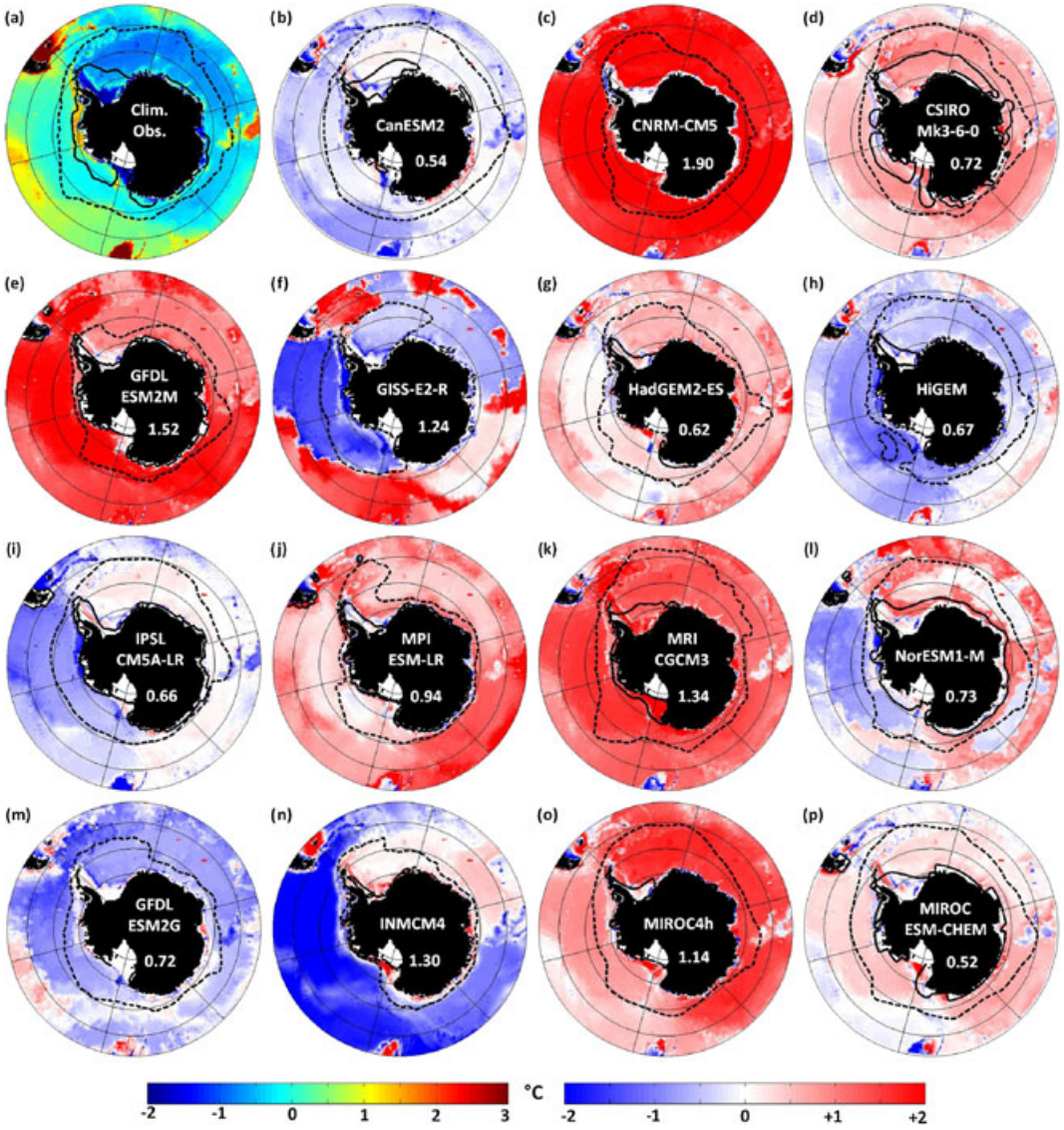

Figure 1. (a) Mean bottom potential temperature of the climatology and (b–p) mean bottom temperature difference (model - climatology); left colorbar corresponds to the climatology, right colorbar to the differences model-climatology (same unit). Thick dashed black line is the mean August sea ice extent (concentration > 15%); thick continuous black line is the mean February sea ice extent (concentration > 15%). Numbers indicate the area-weighted root mean square error for all depths between the model and the climatology (unit °C); mean RMS = 0.97°C.

Deep convection is likely to occur in regions where the mixed-layer extends deeper than half of the whole water column (regions enclosed by the black line on Figure 2). The results are insensitive to the choice of indicator for deep convection. Some models produce dense water by strong deep convection over a large area: GFDL-ESM2M (Figure 2e), GISS-E2-R (Figure 2f) and GFDL-ESM2G (Figure 2m). HadGEM2-ES (Figure 2g), HiGEM (Figure 2h), IPSL-CM5A-LR (Figure 2i) and MPI-ESM-LR (Figure 2j) host deep convection in smaller areas within the Weddell and Ross Gyres, and it is these models, which compare well against the bottom water properties of the climatology.

[14] In contrast, CNRM-CM5 (Figure 2c) and MIROC4h (Figure 2o) have almost no deep convection, and MRI-CGCM3 (Figure 2k) only in the Indian sector but not in the subpolar gyres. These three models develop low-density bottom water (and even lower density surface water) which is too warm, not even producing dense water on the shelf. It might appear that GFDL-ESM2M (Figure 2e) performs similarly, with warm low-density bottom water, but unlike the three other models, it hosts deep convection in the Weddell Gyre. GFDL-ESM2M also has much less winter sea ice than CNRCM-CM5, MRI-CGCM3 and MIROC4h, which may explain the different convective behavior (as we explain below).

[15] CanESM2 (Figure 2b), CSIRO-Mk3-6-0 (Figure 2d), NorESM1-M (Figure 2l), INMCM4 (Figure 2n) and MIROC-ESM-CHEM (Figure 2p) do not host deep convection. They are more saline and/or colder than the other models, and therefore denser at the sea bed, so the ocean is too stratified to convect. Preliminary global

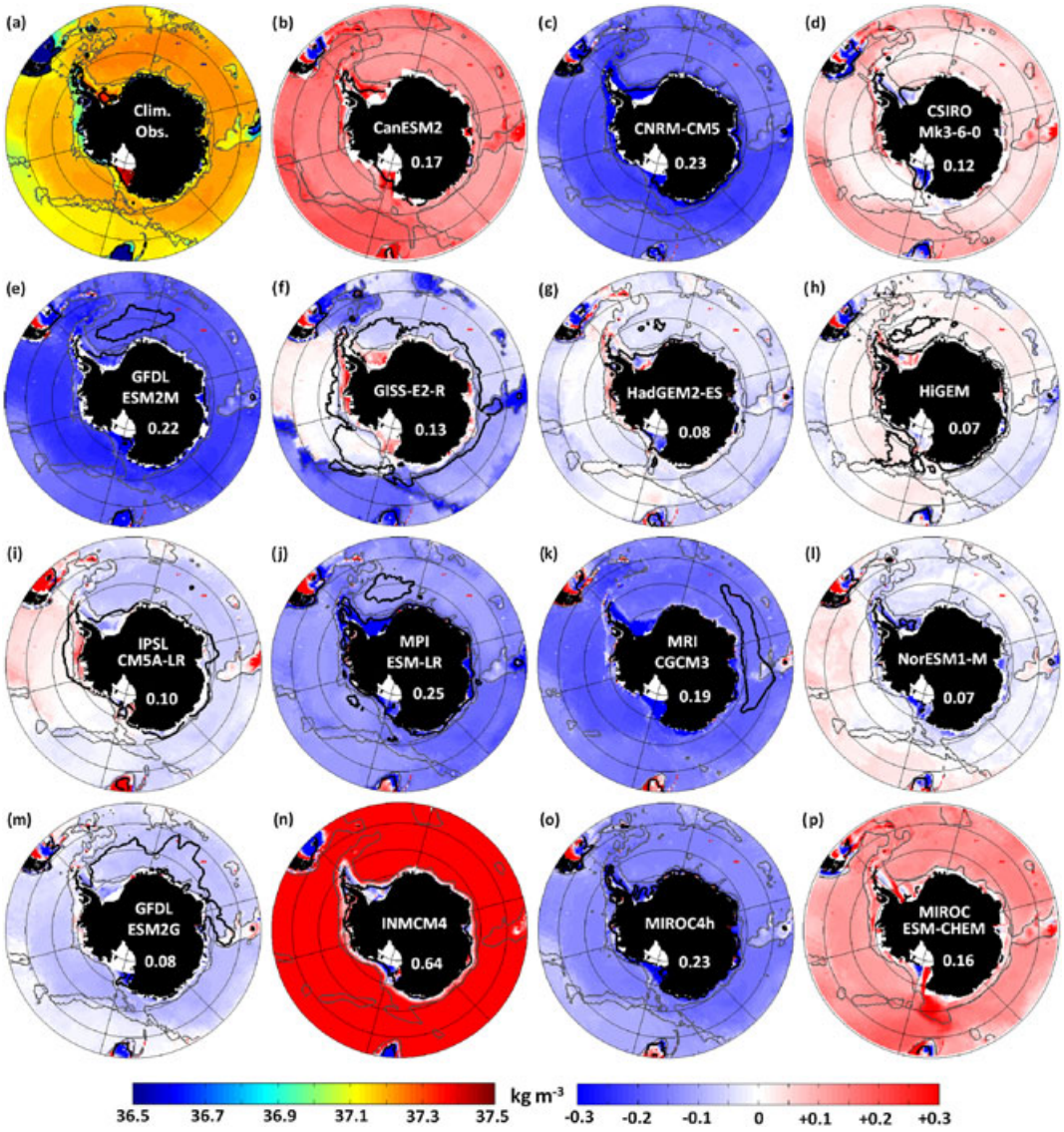

Figure 2. (a) Mean bottom potential density σ_2 of the climatology and (b–p) mean bottom density difference (model - climatology); left colorbar corresponds to the climatology, right colorbar to the differences model-climatology (same unit). Thick black line is the maximum August MLD/bathymetry (quotient > 50%); thin gray line is the 3000 m depth contour. Numbers indicate the area-weighted root mean square error for all depths between the model and the climatology (unit kg m^{-3}); mean RMS = 0.18 kg m^{-3}.

analysis of CanESM2 and INMCM4 (not shown) suggests that their densest water masses originate from the South Atlantic. In contrast, CSIRO-Mk3-6-0, NorESM1-M and MIROC-ESM-CHEM global bottom properties (not shown) indicate that brief open ocean deep convection episodes occur in the Weddell Sea for these models, but a higher temporal resolution than the monthly mean output available would be necessary to observe this process happening.

[16] Some of the different behaviors in the models' bottom water densities can be explained by the models' representation of the seasonal cycle in sea ice extent (black lines on Figure 1). GISS-E2-R (Figure 1f) and GFDL-ESM2G (Figure 1m) have no sea ice left in February and extensive deep convection areas. These models' sea ice needs to be replaced entirely each year, leading to large amounts of brine rejection as the new ice forms, which may cause the vigorous deep convection. Likewise, HadGEM2-ES (Figure 1g), HiGEM (Figure 1h), IPSL-CM5A-LR (Figure 1i) and MPI-ESM-LR (Figure 1j) have less sea ice in February than is observed and host deep convection in the Weddell and Ross Gyres, but as some sea ice remains in February, their deep convection is less intense than for GISS-E2-R and GFDL-ESM2G. In contrast, CanESM2 (Figure 1b), CSIRO-Mk3-6-0 (Figure 1d), MRI-CGCM3 (Figure 1k), NorESM1-M (Figure 1l) and MIROC-ESM-CHEM (Figure 1p) maintain extensive sea ice during summer, and have no deep convection in the subpolar gyres. As the ocean remains covered by sea ice all year long in these models, the mixed-layer is insulated from the cold atmosphere, the brine rejection process is significantly reduced, and no dense water is created by deep convection in the subpolar gyres.

[17] Finally, INMCM4 (Figure 1n) and GFDL-ESM2M (Figure 1e) August sea ice extents exhibit unusual patterns, with very little sea ice respectively in the Ross and Weddell Seas. This could explain why INMCM4 (Figure 2n) is denser than the climatology but does not host deep convection, while GFDL-ESM2M (Figure 2e) is less dense than the climatology but has an extensive area of deep convection. However, it is also possible that these models are exhibiting low frequency variability or are not yet at equilibrium. Trends during the two decades of the study of the area-weighted mean bottom properties (see Table S1) give a decrease of INMCM4's salinity of 0.008 per decade, while GFDL-ESM2M is cooling by 0.013°C per decade. Likewise, CNRM-CM5A (Figure 2c) and MIROC4h (Figure 2o), which both have low-density, warm bottom waters, also have significant cooling trends of 0.02°C per decade.

[18] Of the 15 models in this study, four others have a decreasing bottom temperature trend and their bottom temperature is warmer than the climatology: CSIRO-Mk3-6-0 (-0.011°C/decade), MRI-CGCM3 (-0.010°C/decade), NorESM1-M (–0.022°C/decade) and MIROC-ESM-CHEM (–0.020°C/decade). This suggests that these models exhibit low frequency variability in bottom water properties. In contrast, GISS-E2-R seems to be adjusting to a new climate state: while it is already colder than the climatology in the Weddell and Ross basins, it continues cooling by 0.023°C/decade over the whole Southern Ocean. We note that any model drift (as determined from control runs) has not been removed from the model trends quoted here.

4. Conclusions

[19] Half of the 15 climate models studied here demonstrate an acceptable representation of the water mass properties at the sea bed around Antarctica, with their area-weighted RMS difference from the climatology being lower than the mean of the group of models studied here for bottom temperature, bottom salinity and bottom density. The other half are either too warm or too cold, too salty or too fresh. However, a difference between the modeled bottom waters and the observations can arise because the climate model's ocean state has not fully adjusted from the initial conditions and may never approach an equilibrium state due to some internal long-term trends [*Sen Gupta et al.*, 2012].

[20] Ten of the 15 GCMs produce dense water on the continental shelf, but in none of them can this water spill off the shelf, sink and spread northwards as dense bottom water. For half of the models, deep water is created by deep convection in the open ocean, a mechanism that rarely occurs in the real ocean. However, this mechanism can result in relatively realistic deep water properties. Such convection would have implications for the model carbon and heat uptake by inducing too strong mixing and ventilation, and hence climate sensitivity. Models with extensive deep convection areas (GFDL-ESM2M, GISS-E2-R, MRI-CGCM3 and GFDL-ESM2G) are the ones with a strong seasonal cycle in sea ice: their ocean undergoes a larger heat transfer to the atmosphere, hence cools more, becomes saltier through brine rejection and thus denser.

[21] The three models with the best representations of the sea bed properties (HadGEM2-ES, HiGEM and IPSL-CM5A-LR) are the ones hosting deep convection in the subpolar gyres only. In contrast, models which do not generate deep convection depict poor bottom water properties and are unlikely to lead to accurate predictions of the future state of the deep ocean. Global analyses (not shown) suggest that these models form their deep water either outside of our area of study or through brief deep convection events that we cannot detect with our temporal resolution of monthly average model output.

[22] In this study, no correlation has been found between the models' performances and either their resolution (horizontal or vertical) or the vertical coordinate system (isopycnal, z-level or sigma) used.

[23] No model reproduces the process of Antarctic bottom water formation accurately. Instead of forming dense water on the continental shelf and allowing it to spill off, models present extensive areas of deep convection, thus leading to an unrealistic, unstratified open ocean. Further efforts should be put into a better representation of Antarctic water masses and shelf processes, a key challenge to improve the reliability of climate projections. A grid box model cannot adequately represent the down-slope flow, and it is not clear that higher resolution provides improvements. It is conceivable that a super-parameterization scheme [*Stan et al.*, 2010] might be devised, perhaps based on a high resolution isopycnal model, which would improve the down-slope flow representation. Adaptive meshes and finite element meshes [*Ford et al.*, 2004] could be a solution to model shelf processes at a higher resolution than the open ocean, although they are computationally costly. A simpler solution may be to use tunnels to instantly transport water from the shelf seas to the deep ocean [*Briegleb et al.*, 2010].

[24] **Acknowledgments.** This work is funded by a NERC Open Case award to UEA and the Met Office. Jeff Ridley was supported by the Joint DECC/Defra Met Office Hadley Centre Climate Programme (GA01101). We acknowledge the World Climate Research Programme's Working Group on Coupled Modelling, which is responsible for CMIP, and we thank the climate modeling groups (listed in section 2 of this paper) for producing and making available their model output. For CMIP the U.S. Department of Energy's Program for Climate Model Diagnosis and Intercomparison provides coordinating support and led development of software infrastructure in partnership with the Global Organization for Earth System Science Portals.

References

Briegleb, B. P., G. Danabasoglu, and W. Large, (2010), An overflow parameterization for the ocean component of the Community Climate System Model, *Technical Note NCAR/TN-481+STR*, National Center for Atmospheric Research, Boulder, Colorado.

Chylek, P., J. Li, M. K. Dubey, M. Wang, and G. Lesins (2011), Observed and model simulated 20th century Arctic temperature variability: Canadian Earth System Model CanESM2, *Atmos. Chem. Phys. Discuss.*, *11*(22), 893–907, doi:10.5194/acpd-11-22893-2011.

de Boyer Montégut, C., G. Madec, A. S. Fisher, A. Lazar, and D. Ludicone (2004), Mixed layer depth over the global ocean: An examination of profile data and a profile-based climatology, *J. Geophys. Res.*, *109*, 20, doi: 10.1029/2004JC002378.

Dunne, J. P., et al. (2012), GFDL's ESM2 global coupled climate-carbon Earth System Models Part I: Physical formulation and baseline simulation characteristics, *J. Climate*, *25*, 6646–6665, doi:10.1175/JCLI-D-11-00560.1.

Fofonoff, N. P., and R. C. Millard Jr (1983), *Algorithms for computation of fundamental properties of seawater*, UNESCO/SCOR/ICES/lAPSO Joint Panel on Oceanographic Tables and Standards.

Ford, R., C. C. Pain, M. D. Piggott, A. J. H. Goddard, C. R. E. de Oliveira, and A. P. Umpleby (2004), A nonhydrostatic finite-element model for three-dimensional stratified oceanic flows. Part I: Model formulation, *Mon. Wea. Rev*, *132*, 2816–2831, doi:10.1175/MWR2824.1.

Gordon, H. B., S. P. O'Farrell, M. A. Collier, M. R. Dix, L. D. Rotstayn, E. A. Kowalczyk, A. C. Hirst, and I. G. Watterson, (2010), The CSIRO

Mk3.5 Climate Model, technical report no. 21, *Technical Report 021*, CAWCR, Aspendale, Vic., Australia.

Gouretski, V. V., and K. P. Koltermann, (2004), WOCE Global Hydrographic Climatology, A Technical Report, *Technical Report 35*, BSH, Hamburg, Deutschland.

Hay, W. W. (1993), The role of polar deep water formation in global climate change, *Annu. Rev. Earth Planet. Sci.*, *21*, 227–254, doi:10.1146/annurev.ea.21.050193.001303.

Jones, C. D., et al. (2011), The HadGEM2-ES implementation of CMIP5 centennial simulations, *Geosci. Model Dev.*, *4*, 543–570, doi:10.5194/gmd-4-543-2011.

Jungclaus, J. H., et al. (2010), Climate and carbon-cycle variability over the last millenium, *Clim. of the Past Discuss.*, *6*, 1009–1044, doi:10.5194/cpd-6-1009-2010.

Killworth, P. D. (1983), Deep convection in the world ocean, *Rev. Geophys.*, *21*(1), 1–26, doi:10.1029/RG021i001p00001.

Marshall, J., and F. Schott (1999), Open-ocean convection: Observations, theory and models, *Rev. of Geophys.*, *37*(1), 1–64, doi:10.1209/99/98RG-02739.

Orsi, A. H., G. C. Johnson, and J. L. Bullister (1999), Circulation, mixing, and production of Antarctic Bottom Water, *Prog. Oceanogr.*, *43*, 55–109.

Rayner, N. A., D. E. Parker, E. B. Horton, C. K. Folland, L. V. Alexander, D. P. Rowell, E. C. Kent, and A. Kaplan (2003), Global analyses of sea surface temperature, sea ice, and night marine air temperature since the late nineteenth century, *J. Geophys. Res*, *108*(D14), 4407, doi:10.1029/2002JD002670.

Russell, J. L., R. J. Stouffer, and K. W. Dixon (2006), Intercomparison of the southern ocean circulations in IPCC coupled model control simulations, *J. Climate*, *19*, 4060–4075, doi:10.1175/JCLI3869.1.

Sakamoto, T. T., et al. (2012), MIROC4h—a new high-resolution atmosphere-ocean coupled general circulation model, *J. Meteorol. Soc. Jpn*, *90*(3), 325–359, doi:10.2151/jmsj.2012-301.

Schmidt, G. A., et al. (2006), Present-day atmospheric simulations using GISS ModelE: Comparison to in situ, satellite, and reanalysis data, *J. Climate*, *19*, 153–192, doi:10.1175/JCLI3612.1.

Séférian, R., D. Ludicone, L. Bopp, and G. Madec (2012), Water mass analysis of effect of climate change on air–sea CO2 fluxes: The Southern Ocean, *J. Climate*, *25*, 3894–3908, doi:10.1175/JCLI-D-11-00291.1.

Sen Gupta, A., L. C. Muir, J. N. Brown, S. J. Phipps, P. J. Durack, D. Monselesan, S. E. Wijffels (2012), Climate drift in the CMIP3 Models, *J. Climate*, *25*, 4621–4640, doi:10.1175/JCLI-D-11-00312.1.

Shaffrey, L. C., et al. (2009), U.K. HiGEM: The new U.K. high-resolution global environment model–model description and basic evaluation, *J. Climate*, *22*, 1861–1896, doi:10.1175/2008JCLI2508.1.

Sloyan, B. M., and I. V. Kamenkovich (2007), Simulation of subantarctic mode and Antarctic intermediate waters in climate models, *J. Climate*, *20*, 5061–5080, doi:10.1175/JCLI4295.1.

Stan, C., M. Khairoutdinov, C. A. DeMott, V. Krishnamurthy, D. M. Straus, D. A. Randall, J. L. Kinter III, and J. Shukla (2010), An ocean-atmosphere climate simulation with an embedded cloud resolving model, *Geophys. Res. Lett.*, *37*, L01702, doi:10.1029/2009GL040822.

Taylor, K. E., R. J. Stouffer, and G. A. Meehl (2012), An overview of CMIP5 and the experiment design, *Bull. Amer. Met. Soc.*, *93*, 485–498, doi:10.1175/BAMS-D-11-00094.1.

Tjiputra, J. F., M. Bentsen, C. Roelandt, J. Schwinger, and C. Heinze (2012), Evaluation of the carbon cycle components in the Norwegian Earth System Model (NorESM), *Geosci. Model Dev. Discuss.*, *5*, 3035–3087, doi:10.5194/gmdd-5-3035-2012.

Voldoire, A., et al. (2011), The CNRM-CM5.1 global climate model: Description and basic evaluation, *Clim. Dyn.*, *011*, doi:10.1007/s00382-011-1259-y.

Volodin, E. M., N. A. Dianskii, and A. V. Gusev (2010), Simulating present day climate with the INMCM4.0 coupled model of the atmospheric and oceanic general circulations, *Izv. Atmos. Oceanic Phys.*, *46*(4), 414–431, doi:10.1134/S000143381004002X.

Watanabe, S. et al. (2011), MIROC-ESM: Model description and basic results of CMIP5-20c3m experiments, *Geosci. Model Dev. Discuss.*, *4*, 845–872, doi:10.5194/gmd-4-845-2011.

Yukimoto, S. et al. (2011), A new global climate model of the meteorological research institute: MRI-CGCM3—model description and basic performance, *J. Meteor. Soc.*, *90*(A), 23–64.